IEEE Access
Multidisciplinary | Rapid Review | Open Access Journal

Received November 1, 2021, accepted November 16, 2021, date of publication November 17, 2021,
date of current version November 29, 2021.

Digital Object Identifier 10.1109/ACCESS.2021.3129140

Robust Control Design for an Active Magnetic Bearing System Using Advanced Adaptive SMC Technique

SYED MUHAMMAD AMRR[1], (Graduate Student Member, IEEE), AND ABDULRAHMAN ALTURKI[2]

[1]Department of Electrical Engineering, Indian Institute of Technology Delhi, New Delhi 110016, India
[2]Electrical Engineering Department, College of Engineering, Qassim University, Buraydah 51452, Saudi Arabia

Corresponding author: Syed Muhammad Amrr (syedamrr@gmail.com)

ABSTRACT Fast rotating machines require special attention to ensure accurate rotor placement within the air gap. For this reason, the active magnetic bearings (AMB) system is used to levitate the rotor in the air gap using an electromagnetic feedback control force. The contact-less support AMB system improves the rotor dynamic performance and helps in the success of machine operations. However, the control design for the five degrees-of-freedom (DOF) AMB system is intricate because of its complex nonlinear dynamics. Moreover, these systems are often subjected to model uncertainties, harmonic disturbances, and sensor noises. Therefore, this paper proposes a robust control strategy using an adaptive second-order non-singular fast terminal sliding mode control (SMC) design. The proposed control law employs the higher-order SMC scheme to alleviate the chattering problem from the discontinuous SMC input, which would otherwise restrict its practical applicability. Further, a non-singular fast terminal sliding surface is selected to achieve a faster system response. The adaptive law estimates the switching gain to relax the upper bound assumption of disturbance. The theoretical stability analysis of the proposed methodology proves the finite-time convergence of system states to a small residual bound in the neighborhood of zero. The numerical analysis with a comparative study is also carried out to illustrate the efficacy of the proposed strategy.

INDEX TERMS Uncertain nonlinear system, regulation control, sliding mode control, input chattering, adaptive gain, practical finite-time stability, homogeneity theory, Lyapunov theory.

I. INTRODUCTION

The rotor mass anomaly in a fast rotating machine causes the rotor to vibrate like a harmonic disturbance. Thereby, the rotation of the shaft about its geometric axis creates imbalanced forces. The sources of such discrepancy are undesired electromagnetic forces, external disturbances, model uncertainties, coupling, and gyroscopic effects [1]. Henceforth, the active magnetic bearing (AMB) system is widely used in fast rotating machines to levitate the rotor in the nominal air gap without physical contact. The AMBs balance the rotor displacement using controllable electromagnetic forces and makes the rotor suspension stable [2]. The AMB system is a better alternative to the conventional mechanical bearing system because of the following reasons: no use of lubricants, contact-less support, low maintenance cost, longer life, stable rotor operation at higher speed, strong disturbance rejection capability, faster rotor-dynamic with direct control, adjustable bearings, and small parasitic power loss, etc. Over the past few years, AMBs have been employed in various industrial areas, for instance, in turbo-machinery for oil and gas production, energy-storing flywheels, high-speed electric drives, and many more. [3]–[6].

In recent years, various control methodologies have been employed for the feedback control design of AMB systems. The PID control with updated gains is applied to the AMB system for the rotor stabilization [7], [8]. Gain-scheduling and iterative learning control scheme is presented in [9] for AMBs to compensate for the effects of imbalance over a wide range of rotational speed. In [10], decentralized control is proposed to ensure the high damping and stiffness of the closed-loop AMB system. Other control methods studied for the AMB system are optimal control [11], $\mathcal{H}_\infty$ control [12], fuzzy logic control [13], and the references therein. In the

The associate editor coordinating the review of this manuscript and approving it for publication was Haibin Sun.

above schemes, the controllers are designed under no or less complex uncertainties. So, these control strategies might not provide satisfactory performances in the presence of unknown harmonic disturbances, parametric uncertainties, and sensor noises. Besides, the accurate measurement of rotor speed is also necessary for the practical realization of these control methods.

On the contrary, the sliding mode control (SMC) method is a well-known robust control technique that effectively deals with the matched model uncertainties and disturbances [14]–[16]. The traditional SMC schemes have been explored for the AMB systems that ensure the asymptotic stability [17]–[20]. However, the main issue with the conventional SMC method is the high-frequency switching component called input chattering. The chattering phenomenon can excite the high-frequency components of unmodeled dynamics that may cause damage to the actuator. Moreover, this could also lead to the destabilization of the system response [21], [22]. The simple solution for the chattering problem is the boundary layer technique. In this approach, a continuous approximation function replaces the switching function in the SMC that causes chattering. Although the input chattering is removed through this technique, the invariance property of SMC is compromised, and a true sense of the sliding phase gets lost (i.e., $s \neq 0$). This approach also generates a residual error that is directly dependent upon the width of the boundary layer. Further, the fast unmodeled dynamics of the system are vulnerable under this method which may lead to the unpleasant performance [23], [24]. Inevitably, a compromise is made between allowable chattering and performance accuracy while selecting the thickness of the boundary layer.

A more persuasive method to resolve the problem of chattering without compromising the properties of SMC is the higher-order SMC (HOSMC) technique [25]–[27]. In addition to the alleviation of chattering, the HOSMC yields a better control accuracy than the conventional SMC even under measurement noises and switching delays [28]. The HOSMC scheme has been employed for various applications in [29]–[32]. Lately, it has also been explored for the control of AMBs [1], [33]–[37]. In [33], a super twisting based second-order SMC (SOSMC) scheme is designed for the four degrees-of-freedom (DOF) AMB system. Further, a multivariable continuous SOSMC strategy is presented for the five DOF AMB system [34]. These two schemes stabilize the rotor dynamics under the assumption of a priori upper bound knowledge of disturbance and its derivative, which is not always practically feasible. Moreover, comparison analysis with other methodologies is also not presented to validate their effectiveness. Later, in [34], the assumption about disturbance is relaxed with the use of an adaptive-based SOSMC technique. However, the theoretical analysis only shows the uniformly bounded convergence of sliding surface and adaptation error, while the system states are proved to be asymptotically stable. The SOSMC schemes are also incorporated to design the controller for single DOF AMB and MAGLEV systems [35]–[37]. In these systems, harmonic disturbances are not present because there is no rotatory motion. Hence, the controller design for such a system is more straightforward, and their control designs cannot be generalized for complex systems.

Recently, a composite control using PID and twisting SOSMC method is proposed that guarantees the finite-time stability of the system states [1]. However, the controller is designed based on a priori upper bound knowledge of disturbance. This assumption is relaxed in [27], [38], where adaptive-based integral second and third-order SMC schemes are presented for the AMB system, respectively. Although these schemes prove the finite-time stability of system states, their convergence time is comparatively large, and the input chattering is still evident in the control response of [38].

Considering that the problems of input chattering, dependency on the known bound of disturbance, faster convergence, and finite time stability have not been explored collectively using an advanced SMC scheme. Therefore, this paper employs an adaptive SOSMC method with a non-singular fast terminal sliding surface to stabilize rotor dynamics through five DOF AMBs, which is under the influence of various sources of uncertainties. The main contributions of this work are itemized below.

- This paper investigates the controller design for a five DOF AMB system subjected to multiple challenges such as parametric model uncertainties, external disturbances, and sensor noises. In this regard, a new robust controller is proposed using an adaptive gain-based second-order non-singular fast terminal SMC (ASNFTSMC) design.
- Instead of designing the actual control law, an auxiliary control law is formulated using equivalent and discontinuous control components (which causes chattering). Whereas the actual control input of the system is the time integral of the proposed auxiliary control law. Consequently, due to integration action, the switching component is filtered out from the actual input, and thus chattering problem is attenuated to a great extent.
- The non-singular fast terminal sliding surface is employed in the proposed strategy that gives a faster response and better convergence bound.
- Unlike [1], the switching gain of the proposed method is estimated through an adaptation law that has a dual-rate of adaptation. Consequently, the use of a priori upper bound knowledge of disturbance is averted. Moreover, the dual rate of adaptive law overcomes the problem of overestimation.
- The stability analysis is established through Lyapunov and homogeneity theories that guarantee the practical finite-time stability of the closed-loop system. Hence, the system states converge to a uniform bound in the vicinity of zero within finite time.
- The comparative numerical analysis with the state-of-the-art method shows the effectiveness of the

proposed methodology under various control performance measures.

The rest of the paper is organized in the following way. In Section II, a detailed description of five DOF AMB system is given. Section III presents the problem formulation and devises the proposed control law. In Section IV, stability analysis is conducted using Lyapunov and homogeneity theories, which ensures the practical finite-time stability of sliding variables and state trajectories. Then, Section V discusses the numerical analysis with a comparative study. Lastly, Section VI concludes this paper with a remark on the potential future extensions.

II. MATHEMATICAL MODEL OF THE AMB SYSTEM

A simplified layout of five DOF AMB system is presented in Fig. 1, which comprises a motor, position sensors, one thrust AMB (TAMB) at the middle, and two radial AMBs (RAMBs) at both ends. The RAMBs handle the orientation of four radial DOF, and TAMB takes care of axial orientation. Bearings of the AMB system are made of electromagnetic coils that generate corrective electromagnetic forces to stabilize the rotor suspension using an appropriate feedback control current. The nonlinear attractive electromagnetic forces acting in the directions of X, Y, and Z axes are expressed as [4]

$$F_{x_j} = \alpha \left[\frac{(\bar{i} + i_{x_j})^2}{(\bar{x} - x_j)^2} - \frac{(\bar{i} - i_{x_j})^2}{(\bar{x} + x_j)^2} \right], \tag{1a}$$

$$F_{y_j} = \alpha \left[\frac{(\bar{i} + i_{y_j})^2}{(\bar{y} - y_j)^2} - \frac{(\bar{i} - i_{y_j})^2}{(\bar{y} + y_j)^2} \right], \tag{1b}$$

$$F_z = \alpha \left[\frac{(\bar{i}_t + i_z)^2}{(\bar{z} - z)^2} - \frac{(\bar{i}_t - i_z)^2}{(\bar{z} + z)^2} \right], \tag{1c}$$

where F_{x_j}, F_{y_j}, and F_z are the attractive electromagnetic forces on X, Y, and Z axes with $j = 1, 2$, and α represents the electromagnetic parameter. The terms $\bar{x}$, $\bar{y}$, and $\bar{z}$ denote the nominal air-gap position of rotor in the respective axes, and x_1, y_1, x_2, y_2, and z represent the displacements of rotor in the respective axes. The bias current in the RAMBs of X and Y axes is denoted by $\bar{i}$ and for TAMB, it is expressed by $\bar{i}_t$. The controlling currents for five independent DOF are denoted by i_{x_1}, i_{x_2}, i_{y_1}, i_{y_2}, and i_z.

The Taylor series expansion of the nonlinear electromagnetic forces (1) around a nominal point (i.e., at the origin with zero bias currents) yields the following linearized model [4]

$$F_{x_j}(x_j, i_{x_j}) \cong \alpha_{si}\, i_{x_j} + \alpha_{sp}\, x_j, \tag{2a}$$

$$F_{y_j}(y_j, i_{y_j}) \cong \alpha_{si}\, i_{y_j} + \alpha_{sp}\, y_j, \tag{2b}$$

$$F_z(z, i_z) \cong \alpha_{ti}\, i_z + \alpha_{tp} z, \tag{2c}$$

where α_{sp} and α_{tp} are the respective position stiffness of radial and thrust AMBs and likewise α_{si} and α_{ti} are their current stiffness values.

The rotor deviation dynamics is governed by the state variables $\mathbf{x} = [x_1\ x_2\ y_1\ y_2\ z]^T \in \mathbb{R}^5$. Although the rotor displacement dynamics is a coupled system, the authors of [18], [39] have already developed a decoupled displacement dynamical equation for the five-axis rotor, including a lumped coupling effect term $\mathbf{\Omega} \in \mathbb{R}^5$. Therefore, the decoupled rotor displacement dynamics are expressed as [18]

$$\mathbf{M}\ddot{\mathbf{x}} = \mathbf{A}\mathbf{x} + \mathbf{B}\mathbf{u} + \mathbf{M}\mathbf{\Omega}, \tag{3}$$

where $\mathbf{u} = [i_{x_1}\ i_{x_2}\ i_{y_1}\ i_{y_2}\ i_z]^T \in \mathbb{R}^5$ is the control input and $\mathbf{\Omega} = [\Omega_{x_1}\ \Omega_{x_2}\ \Omega_{y_1}\ \Omega_{y_2}\ \Omega_z]^T$ is the decoupled coupling effect term. The matrices $\mathbf{M} \in \mathbb{R}^{5\times5}$, $\mathbf{A} \in \mathbb{R}^{5\times5}$, and $\mathbf{B} \in \mathbb{R}^{5\times5}$ are the mass matrix, stiffness matrix, and controller gain matrix, respectively and they are defined as [18], [40]

$$\mathbf{M} = \mathbf{I}_{5\times5}, \tag{4}$$

$$\mathbf{A} = \mathrm{diag}(\alpha_{sp}\varpi_1,\ \alpha_{sp}\varpi_3,\ \alpha_{sp}\varpi_1,\ \alpha_{sp}\varpi_3,\ \alpha_{tp}\varpi_4), \tag{5}$$

$$\mathbf{B} = \mathrm{diag}(\alpha_{si}\varpi_1,\ \alpha_{si}\varpi_3,\ \alpha_{si}\varpi_1,\ \alpha_{si}\varpi_3,\ \alpha_{ti}\varpi_4). \tag{6}$$

The coupling effect terms are given as

$$\begin{aligned}
\Omega_{x_1} &= 2\varpi_2(\alpha_{sp}x_2 + \alpha_{si}i_{x2}) + \delta_1(\dot{y}_2 - \dot{y}_1) + \mu_1 f_{dtx},\\
\Omega_{x_2} &= 2\varpi_2(\alpha_{sp}x_1 + \alpha_{si}i_{x1}) + \delta_2(\dot{y}_1 - \dot{y}_2) + \mu_2 f_{dtx},\\
\Omega_{y_1} &= 2\varpi_2(\alpha_{sp}y_2 + \alpha_{si}i_{y2}) + \delta_1(\dot{x}_1 - \dot{x}_2) + \mu_1 f_{dty} - g,\\
\Omega_{y_2} &= 2\varpi_2(\alpha_{sp}y_1 + \alpha_{si}i_{y1}) - \delta_2(\dot{x}_1 + \dot{x}_2) + \mu_2 f_{dty} - g,\\
\Omega_z &= \mu_3 f_{dtz},
\end{aligned} \tag{7}$$

where α_{sp}, α_{tp}, α_{si}, and α_{ti} are constants while $\varpi_1 = (\frac{1}{\mathsf{m}}) + (\frac{\mathsf{a}^2}{J})$, $\varpi_2 = (\frac{1}{\mathsf{m}}) - (\frac{\mathsf{ab}}{J})$, $\varpi_3 = (\frac{1}{\mathsf{m}}) + (\frac{\mathsf{b}^2}{J})$, $\varpi_4 = (\frac{1}{\mathsf{m}})$. Besides, m is the mass of the rotor, a, b, and c are the distance between the center of gravity (CG) and the left RAMB, between CG and the right RAMB, and between CG and the end of the rotor, respectively, and J is the transverse moment of inertia. The terms $\delta_1 = \frac{\mathsf{a}J_z\omega}{Jl}$, $\delta_2 = \frac{\mathsf{b}J_z\omega}{Jl}$, l is the length between both RAMBs, and J_z is the polar moment of inertia. Further, $\mu_1 = (\frac{1}{\mathsf{m}}) - (\frac{\mathsf{ac}}{J})$, $\mu_2 = (\frac{1}{\mathsf{m}}) + (\frac{\mathsf{bc}}{J})$, $\mu_3 = (\frac{1}{\mathsf{m}})$, and f_{dtx}, f_{dty}, and f_{dtz} are the disturbance forces.

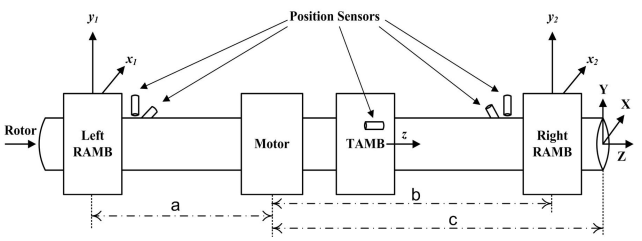

FIGURE 1. Sketch of a five DOF AMB system.

A. CONTROL OBJECTIVE

This paper aims to develop a stabilizing control law for the uncertain AMB system that suspends the rotor inside the nominal air gap. To put it another way, the proposed robust controller must converge the rotor displacement trajectories (x_1, x_2, y_1, y_2, z) to a small neighborhood of zero in finite-time while attenuating the effects of unknown model dynamics and input chattering.

III. PROPOSED CONTROL DESIGN STRATEGY

In this section, the dynamic model of AMB is simplified into a first-order dynamic system with known and unknown parts separated. Later, the proposed control strategy is constituted using the adaptive and SMC techniques.

A. PROBLEM FORMULATION

The mechanical systems often suffer from the variation of system parameters due to wear and tear, aging, and environmental effects. Henceforth, the exact knowledge of system design parameters (e.g., $\mathbf{A}$ and $\mathbf{B}$) is challenging to realize, and there is always some uncertainty involved in the modeling of these parameters. Accordingly, this paper also considers the model uncertainties within the parameters of $\mathbf{A}$ and $\mathbf{B}$ in (3). To further simplify the Equation (3), the effects of these uncertainties can be separated from the nominal part and combined with the coupling effect term. As a result, the dynamical equation (3) is rewritten as [18]

$$\begin{aligned}\ddot{\mathbf{x}} &= (\mathbf{A_0} + \mathbf{A}_{\boldsymbol{\delta}})\mathbf{x}(t) + (\mathbf{B_0} + \mathbf{B}_{\boldsymbol{\delta}})\mathbf{u}(t) + \boldsymbol{\Omega}(t),\\ &= \mathbf{A_0}\mathbf{x}(t) + \mathbf{B_0}\mathbf{u}(t) + \mathbf{d}(t),\end{aligned} \tag{8}$$

where $\mathbf{A_0} \in \mathbb{R}^{5\times5}$, $\mathbf{A}_{\boldsymbol{\delta}} \in \mathbb{R}^{5\times5}$, $\mathbf{B_0} \in \mathbb{R}^{5\times5}$, and $\mathbf{B}_{\boldsymbol{\delta}} \in \mathbb{R}^{5\times5}$ are the corresponding nominal and uncertain components of $\mathbf{A}$ and $\mathbf{B}$, respectively. The time-varying lumped disturbance $\mathbf{d} \in \mathbb{R}^{5\times5}$ comprises of system uncertainties, disturbances, and coupling effect term, and it is described as

$$\mathbf{d}(t) = \mathbf{A}_{\boldsymbol{\delta}}\mathbf{x}(t) + \mathbf{B}_{\boldsymbol{\delta}}\mathbf{u}(t) + \boldsymbol{\Omega}(t). \tag{9}$$

In this paper, the following assumptions are considered while designing the control law for system (8).

Assumption 1: The information of state variable ($\mathbf{x}$) is available for the design of feedback control law.

Assumption 2: The disturbance $\mathbf{d}$ is first order differentiable and bounded, i.e., $\|\dot{\mathbf{d}}\| \leq d_M$ and $\|\mathbf{d}\| \leq d_m$, where the constant values of $d_M > 0$ and $d_m > 0$ are unknown.

Remark 1: The supporting arguments for the Assumption 2 (i.e., boundedness and smoothness of disturbance) are as follows. First of all, the system uncertainty components ($\mathbf{A}_{\boldsymbol{\delta}}$ and $\mathbf{B}_{\boldsymbol{\delta}}$) are always bounded since they are comprised of physical quantities, namely, moment of inertia, mass, length, etc. Secondly, the designed control methodology is based on the SOSMC technique that devises the time derivative of $\mathbf{u}(t)$ as an auxiliary control input $\mathbf{v}(t)$, which is expressed in (19). Consequently, $\dot{\mathbf{u}}(t)$ will always exist under the proposed scheme. Moreover, the electromagnetic coils of AMBs are energized by bounded input current from a rated output power circuit, which can only produce a saturated output. Hence, input $\mathbf{u}(t)$ will also be bounded. Lastly, one can see from (7) that the coupling effect term $\boldsymbol{\Omega}(t)$ includes state variables, constant coefficients, control inputs, gravitational force, and sinusoidal exogenous disturbance. Since all these functions are bounded and first-order differentiable; therefore, $\boldsymbol{\Omega}(t)$ is also finite and continuous [18], [41]. This implies all the terms within (9) are bounded and differentiable.

The system dynamics (8) can also be expressed in terms of first-order differential equations by selecting the following new sets of variables:

$$\begin{aligned}\mathbf{x}_1 &= \mathbf{x} \in \mathbb{R}^5,\\ \mathbf{x}_2 &= \dot{\mathbf{x}} \in \mathbb{R}^5.\end{aligned} \tag{10}$$

Substituting (10) in the dynamics of (8) yields

$$\begin{aligned}\dot{\mathbf{x}}_1 &= \mathbf{x}_2(t),\\ \dot{\mathbf{x}}_2 &= \mathbf{A_0}\mathbf{x}_1(t) + \mathbf{B_0}\mathbf{u}(t) + \mathbf{d}(t).\end{aligned} \tag{11}$$

Therefore, the control objective is to converge the states $\mathbf{x}_1(t)$ and $\mathbf{x}_2(t)$ in the neighborhood of zero within finite time.

B. PROPOSED ADAPTIVE SECOND-ORDER NON-SINGULAR FAST TERMINAL SMC DESIGN

Consider a sliding variable $\boldsymbol{\sigma} \in \mathbb{R}^5$, which is defined as

$$\boldsymbol{\sigma} = \mathbf{x}_1. \tag{12}$$

From the system dynamics (11), the subsequent time derivatives of $\boldsymbol{\sigma}$ yields

$$\dot{\boldsymbol{\sigma}} = \dot{\mathbf{x}}_1 = \mathbf{x}_2(t), \tag{13a}$$

$$\ddot{\boldsymbol{\sigma}} = \dot{\mathbf{x}}_2 = \mathbf{A_0}\mathbf{x}_1(t) + \mathbf{B_0}\mathbf{u}(t) + \mathbf{d}(t), \tag{13b}$$

$$\dddot{\boldsymbol{\sigma}} = \ddot{\mathbf{x}}_2 = \mathbf{A_0}\mathbf{x}_2(t) + \mathbf{B_0}\mathbf{v}(t) + \mathbf{D}(t), \tag{13c}$$

where the auxiliary input, $\mathbf{v}(t) = \dot{\mathbf{u}}(t) \in \mathbb{R}^5$ and $\mathbf{D}(t) = \dot{\mathbf{d}}(t) \in \mathbb{R}^5$.

Remark 2: Since $\mathbf{u}(t)$ appears in the second derivative of $\boldsymbol{\sigma}$, the sliding variable has a relative degree 2.

With the use of sliding variable $\boldsymbol{\sigma}$ and its time derivatives, a non-singular fast terminal sliding manifold $\mathbf{s} \in \mathbb{R}^5$ is proposed as

$$\mathbf{s} = \ddot{\boldsymbol{\sigma}} + \lambda_1 \lceil \boldsymbol{\sigma} \rfloor^{\rho_1} + \lambda_2 \lceil \dot{\boldsymbol{\sigma}} \rfloor^{\rho_2}, \tag{14}$$

where $\lambda_1 > 0$, $\lambda_2 > 0$ are control design constants, $\rho_1 \in (0, 1)$, $\rho_2 \in (0, 1)$, and the operator $\lceil \boldsymbol{\sigma} \rfloor^{\rho}$ is expressed as

$$\lceil \boldsymbol{\sigma} \rfloor^{\rho} = [\mathrm{sign}(\sigma_1)|\sigma_1|^{\rho}, \cdots, \mathrm{sign}(\sigma_5)|\sigma_5|^{\rho}]^T \in \mathbb{R}^5. \tag{15}$$

The time derivative of (14) using (13) yields

$$\begin{aligned}\dot{\mathbf{s}} &= \dddot{\boldsymbol{\sigma}} + \lambda_1\rho_1 \mathrm{diag}(|\boldsymbol{\sigma}|^{(\rho_1-1)})\dot{\boldsymbol{\sigma}} + \lambda_2\rho_2 \mathrm{diag}(|\dot{\boldsymbol{\sigma}}|^{(\rho_2-1)})\ddot{\boldsymbol{\sigma}},\\ &= (\mathbf{A_0}\mathbf{x}_2 + \mathbf{B_0}\mathbf{v} + \mathbf{D}) + \lambda_1\rho_1 \mathrm{diag}(|\boldsymbol{\sigma}|^{(\rho_1-1)})\mathbf{x}_2\\ &\quad + \lambda_2\rho_2 \mathrm{diag}(|\dot{\boldsymbol{\sigma}}|^{(\rho_2-1)})(\mathbf{A_0}\mathbf{x}_1 + \mathbf{B_0}\mathbf{u} + \mathbf{d}),\\ &= \mathcal{F}(\mathbf{x}_1, \mathbf{x}_2, \mathbf{u}) + \mathbf{B_0}\mathbf{v} + \mathcal{D}(\mathbf{D}, \mathbf{d}),\end{aligned} \tag{16}$$

where

$$\begin{aligned}\mathcal{F}(\cdot) &= \mathbf{A_0}\mathbf{x}_2 + \lambda_2\rho_2 \mathrm{diag}(|\dot{\boldsymbol{\sigma}}|^{(\rho_2-1)})(\mathbf{A_0}\mathbf{x}_1 + \mathbf{B_0}\mathbf{u})\\ &\quad + \lambda_1\rho_1 \mathrm{diag}(|\boldsymbol{\sigma}|^{(\rho_1-1)})\mathbf{x}_2,\end{aligned} \tag{17}$$

$$\mathcal{D}(\cdot) = \mathbf{D} + \lambda_2\rho_2 \mathrm{diag}(|\dot{\boldsymbol{\sigma}}|^{(\rho_2-1)})\mathbf{d}. \tag{18}$$

From (16), the obvious choice for the control $\mathbf{v}$ is

$$\mathbf{v} = \mathbf{B_0}^{-1}\left(-\mathcal{F}(\cdot) - \beta\mathbf{s} - \hat{k}\,\mathrm{sign}(\mathbf{s})\right), \tag{19}$$

where $\beta > 0$ is a constant gain, $\hat{k}$ is a time-varying adaptive gain whose governing equation is inspired from [42], [43] and it is defined as

$$\dot{\hat{k}} = \begin{cases} \bar{k}\|\mathbf{s}\|\text{sign}(\|\mathbf{s}\| - \bar{\epsilon}) & \text{if } \hat{k} = \bar{\mu} \\ \bar{\mu} & \text{if } \hat{k} \leq \bar{\mu} \end{cases} \tag{20}$$

where $\hat{k}(0)$, $\bar{k}$, $\bar{\epsilon}$, and $\bar{\mu}$ are all positive parameters, which are to be selected. The parameter $\bar{\mu}$ helps in restricting the adaptive gain $\hat{k}(t)$ from reaching to a negative value. Therefore, a strong condition would be $\hat{k}(t) > \bar{\mu}\ \forall\ t > 0$. Moreover, to limit the unbounded increase in the value of gain $\hat{k}(t)$, parameter $\bar{\epsilon}$ is employed. This will stop further increment in $\hat{k}(t)$ when the sliding surface approaches the region around $\bar{\epsilon}$, because an ideal sliding mode with absolute $\mathbf{s} = 0$ is not possible in a real-time applications.

Remark 3: The auxiliary control (19) employs the sliding surface $\mathbf{s}$ that requires the information of $\dot{\boldsymbol{\sigma}}$ and $\ddot{\boldsymbol{\sigma}}$, i.e., $\dot{\mathbf{x}}_1$ and $\ddot{\mathbf{x}}_1$. These measurements can be obtained by employing the Levant's 2^{nd} order exact robust finite-time differentiator [25]. The Levant's differentiator determines the time derivatives of input variable. Therefore, the known input variable $\boldsymbol{\sigma}$ under this methodology gives the output $\dot{\boldsymbol{\sigma}}$ and $\ddot{\boldsymbol{\sigma}}$. The Levant's 2^{nd} order differentiator takes the following form [25]

$$\dot{\boldsymbol{\varphi}}_0 = \mathbf{w}_0 = -\eta_0 \lceil \boldsymbol{\varphi}_0 - \boldsymbol{\sigma} \rfloor^{\frac{2}{3}} + \boldsymbol{\varphi}_1, \tag{21a}$$

$$\dot{\boldsymbol{\varphi}}_1 = \mathbf{w}_1 = -\eta_1 \lceil \boldsymbol{\varphi}_1 - \mathbf{w}_0 \rfloor^{\frac{1}{2}} + \boldsymbol{\varphi}_2, \tag{21b}$$

$$\dot{\boldsymbol{\varphi}}_2 = -\eta_2\ \text{sign}(\boldsymbol{\varphi}_2 - \mathbf{w}_1), \tag{21c}$$

where $\boldsymbol{\varphi}_0$, $\boldsymbol{\varphi}_1$, and $\boldsymbol{\varphi}_2 \in \mathbb{R}^5$ are the real-time estimates of $\boldsymbol{\sigma}$, $\dot{\boldsymbol{\sigma}}$, and $\ddot{\boldsymbol{\sigma}}$, respectively, and the parameters η_0, $\eta_1 > 0$, and $\eta_2 > 0$ are all positive constants.

IV. STABILITY ANALYSIS

The following Lemmas are adopted to establish the stability proof of the closed-loop system.

Lemma 1 [44]: Consider a system

$$\dot{\boldsymbol{\vartheta}} = \boldsymbol{f}(\boldsymbol{\vartheta}) \in \mathbb{R}^n,\ \boldsymbol{\vartheta}(t_0) = \boldsymbol{\vartheta}_0,\ \boldsymbol{f}(t_0) = 0 \text{ and } t_0 = 0, \tag{22}$$

where $\boldsymbol{f}(\boldsymbol{\vartheta})$ is continuous. Suppose there exist a Lyapunov function $\mathcal{V}(\boldsymbol{\vartheta}) : \mathbb{R}^n \to \mathbb{R}$ with $\beta > 0$ and $\gamma \in (0, 1)$, such that

$$\dot{\mathcal{V}}(\boldsymbol{\vartheta}) \leq -\beta \mathcal{V}^{\gamma}(\boldsymbol{\vartheta}). \tag{23}$$

Then, the origin is a finite-time stable point for (22) and the settling time of state $\boldsymbol{\vartheta}(t)$ is given as $T_{\text{settling}} \leq \frac{\mathcal{V}^{1-\gamma}(\boldsymbol{\vartheta}_0)}{\beta(1-\gamma)}$.

Lemma 2 [45]: Considering the same scenario of Lemma 1 with a bounded set $\phi > 0$. Now, if the given inequality is satisfied

$$\dot{\mathcal{V}}(\boldsymbol{\vartheta}) \leq -\beta \mathcal{V}^{\gamma}(\boldsymbol{\vartheta}) + \phi, \tag{24}$$

then, the system states of (22) are practically finite-time stable (PFS). Moreover, given a scalar $\lambda \in (0, 1]$, the state trajectories $\boldsymbol{\vartheta}$ converge to a small bound in a finite time, which is defined as

$$\lim_{\lambda \to \lambda_0} \boldsymbol{\vartheta} \in \mathcal{V}^{\gamma}(\boldsymbol{\vartheta}) \leq \left(\frac{\phi}{(1-\lambda)\beta} \right), \tag{25}$$

where $\lambda_0 \in (0, 1)$, and $T_{\text{settling}} \leq \frac{\mathcal{V}^{1-\gamma}(\boldsymbol{\vartheta}_0)}{\beta\lambda_0(1-\gamma)}$.

Lemma 3 [42]: Given the sliding dynamics (16) and the adaptation law (20), the switching gain $\hat{k}$ has an upper bound, i.e., $\exists$ a non-negative constant k such that

$$\hat{k}(t) \leq k, \forall\ t > 0. \tag{26}$$

A. CONVERGENCE OF SLIDING SURFACE, s

Theorem 1: Consider the sliding dynamics (16) under Assumption 2. The proposed auxiliary control (19) guarantees the practical finite-time convergence of sliding manifold to a small bound in the vicinity of zero.

Proof: In this Theorem, the Lyapunov theory is used to demonstrate the convergence of $\mathbf{s}$. On the other hand, the subsequent Theorem will establish the convergence of state trajectories by employing the homogeneity theory.

Consider a Lyapunov candidate function V_1 as

$$V_1 = \frac{1}{2}\mathbf{s}^T\mathbf{s} + \frac{1}{2\theta}(\hat{k} - k)^2, \tag{27}$$

where $\tilde{k} = \hat{k} - k$ is the adaptive estimation error, k is an unknown constant such that $k > \|\mathcal{D}\| = \mathcal{D}_{\max}$, and $\theta > 0$ decides the rate of adaptation. Time derivative of (27) yields

$$\dot{V}_1 = \mathbf{s}^T\dot{\mathbf{s}} + \frac{1}{\theta}(\hat{k} - k)\dot{\hat{k}}. \tag{28}$$

Substituting (16) into (28) gives

$$\dot{V}_1 = \mathbf{s}^T(\mathcal{F} + \mathbf{B_0}\mathbf{v} + \mathcal{D}) + \frac{1}{\theta}(\hat{k} - k)\dot{\hat{k}}. \tag{29}$$

Incorporating the auxiliary control law (19) in (29), and after simplification it results in

$$\begin{aligned} \dot{V}_1 &= \mathbf{s}^T(-\beta\mathbf{s} - \hat{k}\text{sign}(\mathbf{s}) + \mathcal{D}) + \frac{1}{\theta}(\hat{k} - k)\dot{\hat{k}}, \\ &\leq -\beta\|\mathbf{s}\|^2 - \hat{k}\|\mathbf{s}\| + \mathcal{D}_{\max}\|\mathbf{s}\| + \frac{1}{\theta}(\hat{k} - k)\dot{\hat{k}}. \end{aligned} \tag{30}$$

Adding and subtracting a term $k\|\mathbf{s}\|$ in (30) and substituting (20) gives

$$\begin{aligned} \dot{V}_1 &\leq -\hat{k}\|\mathbf{s}\| + k\|\mathbf{s}\| - k\|\mathbf{s}\| + \mathcal{D}_{\max}\|\mathbf{s}\| + (\hat{k} - k)\frac{\bar{k}}{\theta}\|\mathbf{s}\| \\ &\quad \times \text{sign}(\|\mathbf{s}\| - \bar{\epsilon}), \\ &= -(k - \mathcal{D}_{\max})\|\mathbf{s}\| - (\hat{k} - k)\|\mathbf{s}\| + (\hat{k} - k)\frac{\bar{k}}{\theta}\|\mathbf{s}\| \\ &\quad \times \text{sign}(\|\mathbf{s}\| - \bar{\epsilon}), \\ &= -k_d\|\mathbf{s}\| + (\hat{k} - k)\left(-\|\mathbf{s}\| + \frac{\bar{k}}{\theta}\|\mathbf{s}\|\text{sign}(\|\mathbf{s}\| - \bar{\epsilon}) \right), \end{aligned}$$

where $k_d = (k - \mathcal{D}_{\max}) > 0$ because $k > \|\mathcal{D}\| = \mathcal{D}_{\max}$. Now, introducing a positive term $\zeta_k > 0$ as

$$\begin{aligned} \dot{V}_1 = -k_d\|\mathbf{s}\| - \zeta_k\|\hat{k} - k\| + \zeta_k\|\hat{k} - k\| \\ + (\hat{k} - k)\left(-\|\mathbf{s}\| + \frac{\bar{k}}{\theta}\|\mathbf{s}\|\text{sign}(\|\mathbf{s}\| - \bar{\epsilon}) \right). \end{aligned} \tag{31}$$

From Lemma 3, $\exists\ k$ such that $(\hat{k} - k) < 0\ \forall\ t > 0$. Implementing this result in (31) gives

$$\dot{V}_1 = -k_d\|\mathbf{s}\| - \zeta_k\|\hat{k} - k\| - \left(-\|\mathbf{s}\| + \frac{\bar{k}}{\theta}\|\mathbf{s}\|\text{sign}(\|\mathbf{s}\| - \bar{\epsilon}) - \zeta_k \right)$$

$$\times \|\hat{k}-k\|,$$
$$= -k_d\|\mathbf{s}\| - \zeta_k\|\hat{k}-k\| - \Phi, \tag{32}$$

where $\Phi = \left(-\|\mathbf{s}\| + \frac{\bar{k}}{\theta}\|\mathbf{s}\|\text{sign}(\|\mathbf{s}\| - \bar{\epsilon}) - \zeta_k\right)\|\hat{k} - k\|$. Rewriting Equation (32) as

$$\begin{aligned}\dot{V}_1 &= -k_d\sqrt{2}\frac{\|\mathbf{s}\|}{\sqrt{2}} - \zeta_k\sqrt{2\theta}\frac{\|\hat{k}-k\|}{\sqrt{2\theta}} - \Phi,\\ &\leq -\min(k_d\sqrt{2}, \zeta_k\sqrt{2\theta})\left(\frac{\|\mathbf{s}\|}{\sqrt{2}} + \frac{\|\hat{k}-k\|}{\sqrt{2\theta}}\right) - \Phi,\\ &\leq -\gamma V_1^{1/2} - \Phi, \end{aligned}\tag{33}$$

where $\gamma = \sqrt{2}\min(k_d, \zeta_k\sqrt{\theta}) > 0$. The polarity of variable Φ and the subsequent stability analysis depends on the condition of $\|\mathbf{s}\|$. Therefore, the following two cases are discussed:

Case (i). When $\|\mathbf{s}\| > \bar{\epsilon}$. In this case, Φ is positive if

$$\begin{aligned}-\|\mathbf{s}\| + \frac{\bar{k}}{\theta}\|\mathbf{s}\| - \zeta_k > 0,\\ \Rightarrow \theta < \frac{\bar{k}\bar{\epsilon}}{\zeta_k + \bar{\epsilon}}.\end{aligned}\tag{34}$$

With Φ being positive under this scenario, the derivative of Lyapunov function from (33) yields

$$\dot{V}_1 \leq -\gamma V_1^{1/2}. \tag{35}$$

Therefore, according to Lemma 1, $\mathbf{s}$ will converge to the bound $\bar{\epsilon}$ within a finite time.

Case (ii). When $\|\mathbf{s}\| \leq \bar{\epsilon}$. Under this scenario, Φ can be negative, and thus, Equation (33) is written as

$$\dot{V}_1 \leq -\gamma V_1^{1/2} + \Phi. \tag{36}$$

The above inequality (36) satisfies the practically finite time stability condition given in Lemma 2. This implies that $\|\mathbf{s}\|$ reaches the region $\bar{\epsilon}$ in finite time. However, the behaviour of $\|\mathbf{s}\|$ inside the bound of $\bar{\epsilon}$ can not be ascertained.

Moreover, suppose at some point of time (say t_{F1}) if the sliding manifold escapes from the region $\bar{\epsilon}$, i.e., $\|\mathbf{s}(t_{F1})\| > \bar{\epsilon}$. Then, there always exists another finite time t_{F2} when $\|\mathbf{s}\|$ will re-enter inside the region $\bar{\epsilon}$. Hence, this establishes that the variable $\mathbf{s}$ achieves a real sliding mode. □

B. CONVERGENCE OF STATE VARIABLES, $\mathbf{x_1}$ & $\mathbf{x_2}$

As the sliding surface $\mathbf{s}$ converges into a small set $\bar{\epsilon}$ around the origin, the analysis of the state trajectories is demonstrated through the following steps.

When real sliding mode is attained, i.e., $\|\mathbf{s}\| < \bar{\epsilon}$, finite time convergence of $\mathbf{x}_1$ and $\mathbf{x}_2$ is guaranteed. This fact can also be established through the sliding variable dynamics from (14) as [46]

$$\ddot{\boldsymbol{\sigma}} + \lambda_1\lceil\boldsymbol{\sigma}\rfloor^{\rho_1} + \lambda_2\lceil\dot{\boldsymbol{\sigma}}\rfloor^{\rho_2} < \boldsymbol{\varepsilon}, \tag{37}$$

where $\boldsymbol{\varepsilon}(t) \in \mathbb{R}^5$ such that $\|\boldsymbol{\varepsilon}(t)\| \leq \bar{\epsilon}$. Similar to the notion given in [47], Equation (37) can be redefined in the first order derivatives using (11), (12), and (13) as

$$\dot{\mathbf{x}}_1 = \mathbf{x}_2, \tag{38a}$$

$$\dot{\mathbf{x}}_2 = -\lambda_1\lceil\mathbf{x}_1\rfloor^{\rho_1} - \lambda_2\lceil\mathbf{x}_2\rfloor^{\rho_2} + \boldsymbol{\varepsilon}. \tag{38b}$$

Remark 4: The reduced closed-loop dynamic Equation (38) is in the form of a double integrator system. Now, by selecting the parameters ρ_1 and ρ_2 such that

$$\rho_1 = \frac{\rho_2\rho_3}{2\rho_3 - \rho_2}, \quad \text{where} \quad \rho_3 = 1, \tag{39}$$

then, the proposed Equation (38) becomes equivalent to the condition presented in the proof of Theorem 2 in [47]. Consequently, the states $\mathbf{x}_1$ and $\mathbf{x}_2$ will converge to an invariant set within finite time.

Theorem 2: Consider the reduced system dynamics (38) when the real sliding mode phase is obtained ($\|\mathbf{s}\| \leq \bar{\epsilon}$). Under the given scenario, the system state trajectories steered to the neighborhood of origin in finite-time, and their residual bounds are

$$\|\mathbf{x}_1\| \leq \left(\frac{\lambda_2\xi(1+\rho_1)}{\lambda_1}\right)^{\frac{1}{1+\rho_1}}, \ \|\mathbf{x}_2\| \leq \left(\frac{\bar{\epsilon}}{\lambda_2}\right)^{1/\rho_2}, \tag{40}$$

where $\xi > 0$ is defined later.

Proof: The proposition for the finite-time stability of chain integrator system with n^{th} order dynamics using homogeneity theory, without the $\bar{\epsilon}$ bound, has already been presented in [48]. Further, in [47], the preceding result is extended for the system with a narrow convergence bound, like $\boldsymbol{\varepsilon}$ in (38). Accordingly, two steps are required to guarantee the finite-time stability of such a dynamical system. These steps include two affirmations: (i) asymptotic stability of the system (38), and (ii) negative degree of homogeneity of the associated vector field.

The first part of the proof can easily be presented using the following Lyapunov function

$$V_2(\mathbf{x}_1, \mathbf{x}_2) = \frac{\lambda_1}{\lambda_2}\frac{1}{1+\rho_1}|\mathbf{x}_1|^{1+\rho_1} + \frac{1}{2\lambda_2}\mathbf{x}_2^T\mathbf{x}_2. \tag{41}$$

Note that $\frac{d}{dt}|\mathbf{x}_1|^{1+\rho_1} = (1+\rho_1)\lceil\mathbf{x}_1\rfloor^{\rho_1}\dot{\mathbf{x}}_1$ [38]. Therefore, substituting this fact in the time derivative of V_2 gives

$$\dot{V}_2(\mathbf{x}_1, \mathbf{x}_2) = \frac{\lambda_1}{\lambda_2}|\mathbf{x}_1|^{\rho_1}\text{sign}(\mathbf{x}_1)\dot{\mathbf{x}}_1 + \frac{1}{\lambda_2}\mathbf{x}_2^T\dot{\mathbf{x}}_2 \tag{42}$$

Substituting (38) into (42) yields

$$\begin{aligned}\dot{V}_2 &= \frac{\lambda_1}{\lambda_2}\mathbf{x}_2^T\lceil\mathbf{x}_1\rfloor^{\rho_1} + \frac{1}{\lambda_2}\mathbf{x}_2^T(-\lambda_1\lceil\mathbf{x}_1\rfloor^{\rho_1} - \lambda_2\lceil\mathbf{x}_2\rfloor^{\rho_2} + \boldsymbol{\varepsilon})\\ &\leq -|\mathbf{x}_2|^{\rho_2+1} + \frac{1}{\lambda_2}\|\mathbf{x}_2\|\|\boldsymbol{\varepsilon}\|\\ &\leq -|\mathbf{x}_2|^{\rho_2+1} + \frac{1}{\lambda_2}\bar{\epsilon}\|\mathbf{x}_2\|.\end{aligned}\tag{43}$$

For $\dot{V}_2$ to be negative definite, i.e., $\dot{V}_2 < 0$, the condition $|\mathbf{x}_2|^{\rho_2} > \bar{\epsilon}/\lambda_2$ must be satisfied. Suppose, the minimum value that V_2 can achieve be given by $\wp_{\min}$, which means

$$|\mathbf{x}_1|^{1+\rho_1} = \frac{1+\rho_1}{\lambda_1}\left(\lambda_2\wp_{\min} - \frac{1}{2}\left(\frac{\bar{\epsilon}}{\lambda_2}\right)^{2/\rho_2}\right). \tag{44}$$

Now, for $|\mathbf{x}_1|^{1+\rho_1}$ to exist in the real space $\mathbb{R}$, $\wp_{\min}$ should satisfy

$$\wp_{\min} > \frac{1}{2\lambda_2}\left(\frac{\bar{\epsilon}}{\lambda_2}\right)^{2/\rho_2}. \tag{45}$$

Moreover, if $\wp_{\min} = \frac{1}{2\lambda_2}\left(\frac{\bar{\epsilon}}{\lambda_2}\right)^{2/\rho_2}$ is achieved, then $|\mathbf{x}_1|$ converges to zero in finite time, which ultimately means the asymptotic stability is guaranteed. Hence, the invariant set of system states become

$$\psi_1 = \left\{(\mathbf{x}_1, \mathbf{x}_2) \in \mathbb{R}^5 \,\middle|\, \|\mathbf{x}_1\| = 0, \|\mathbf{x}_2\| \leq \left(\frac{\bar{\epsilon}}{\lambda_2}\right)^{\frac{1}{\rho_2}}\right\}. \tag{46}$$

Another aspect is also possible when the given value of $\wp_{\min}$ is not achieved in a finite time. Accordingly, the invariant set of the closed-loop system is modified as follows.

Define a variable $\xi > 0$ that represents the difference in the instantaneous and steady-state values of $\wp_{\min}$. By following the steps given in [47], the revised invariant set of system state is

$$\psi_2 = \left\{\|\mathbf{x}_1\| \leq \left(\frac{\lambda_2\xi(1+\rho_1)}{\lambda_1}\right)^{\frac{1}{1+\rho_1}}, \|\mathbf{x}_2\| \leq \left(\frac{\bar{\epsilon}}{\lambda_2}\right)^{\frac{1}{\rho_2}}\right\}. \tag{47}$$

Hence, the asymptotic convergence of the closed-loop system to the above invariant set is guaranteed. Thus, the first condition for finite-time stability is fulfilled.

Now, the second part of the proof, i.e., negative homogeneity of the associated vector field, can be easily ensured by adopting the simple steps given in [47]. For brevity and to avoid repetition, this part of the proof is omitted from here.

Therefore, in view of Remark 4 and the above analysis, the finite-time stability of the dynamical system (38) to a residual set ψ_2 is guaranteed. Henceforth, the proof of Theorem 2 is completed. □

Figure 2 presents the schematic diagram of the proposed control methodology for 5 DOF AMB system.

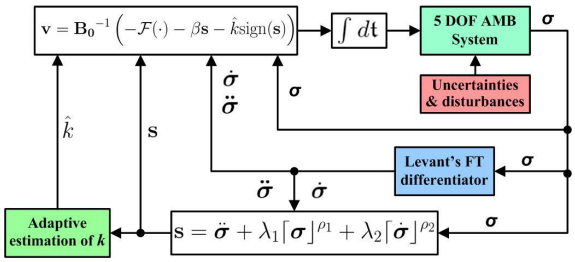

FIGURE 2. Block diagram of the proposed control algorithm.

V. NUMERICAL ANALYSIS

This section presents the numerical results of the proposed adaptive second-order non-singular fast terminal SMC (ASNFTSMC) (19) for the uncertain AMB system. The comparative analysis with a recently developed adaptive integral SOSMC (AISOSMC) scheme [38] is also demonstrated to illustrate the effectiveness of the proposed strategy.

The various physical parameters of the five DOF AMB system is given in Table 1, and these values are taken from [18], [41]. In order to suspend and neutralize the weight of the rotor, the following bias DC currents are supplied in the RAMB and TAMB coils: $\bar{i} = 0.9$ A and $\bar{i}_t = 1.1$ A. The nominal air gap of RAMB and TAMB (i.e., $(\bar{x}, \bar{y})$ and $\bar{z}$) is selected as 0.4 mm and 0.5 mm, respectively. The sources of uncertainties in AMB is considered from uncertain system parameters, disturbances, and noises. Therefore, the system model uncertainties, i.e., $\mathbf{A}_{\boldsymbol{\delta}}$ and $\mathbf{B}_{\boldsymbol{\delta}}$, are chosen as 15% and 20% of their respective nominal values. Further, the external disturbance forces is taken as

$$\begin{bmatrix} f_{dtx} \\ f_{dty} \\ f_{dtz} \end{bmatrix} = \begin{bmatrix} 0.1\sin(t) \\ 0.2\sin(5t) \\ 0.3\sin(8t) \end{bmatrix} + 0.05\boldsymbol{\eta},$$

where $\boldsymbol{\eta} \in \mathbb{R}^3$ is the white noise. Moreover, random Gaussian noise of amplitude 1×10^{-4} mm is also selected as a sensor noise in the closed loop system to determine the effectiveness of the control strategies under noisy measurements.

TABLE 1. Design parameters of the given AMB system [18], [41].

Parameter	Value	Parameter	Value
Rotor length (L)	0.505 m	J	0.04004 kg.m^2
Rotor diameter (d)	0.0166 m	J_z	0.0006565 kg.m^2
m	2.56478 kg	α_{ti}	40 N/A
a	0.16 m	α_{tp}	36000 N/m
b	0.19 m	α_{si}	80 N/A
c	0.263 m	α_{sp}	220000 N/m
l	0.35 m	ω_{rated}	2400 rpm

The initial conditions of the rotor position are chosen as

$$\mathbf{x}(0) = \begin{bmatrix}0.3 & 0.1 & 0.2 & 0.15 & 0.4\end{bmatrix}^T \text{mm}.$$

The control parameters of the proposed scheme (19) and the comparative algorithm are given in Table 2. The following subsection presents the simulation performance of both control strategies for the comparative analysis.

TABLE 2. Parameters of both control schemes.

Schemes	Parameters
ASNFTSMC	$\beta = 4000, \rho_1 = 3/5, \hat{k}(0) = 0.01, \eta_0 = 3$
	$\lambda_1 = 0.95, \rho_2 = 3/4, \bar{\epsilon} = 1.5 \times 10^{-3}, \eta_1 = 1.5$
	$\lambda_2 = 0.6, k = 150, \bar{\mu} = 1 \times 10^{-4}, \eta_2 = 1.1$
AISOSMC [38]	$K_1 = 180, \gamma_1 = 0.5, \xi = 0.001, \hat{\alpha}(0) = 400$
	$K_2 = 350, \delta = 3 \times 10^{-3}, \varrho = 80, \hat{\beta}(0) = 0$

A. COMPARATIVE PERFORMANCE RESULTS

The performance of the proposed and comparative control strategies are illustrated in Fig. 3–12 for the duration of 1.5s. The time response of rotor displacement from the unbalanced initial position to the nominal air gap position (i.e., origin) is presented in Fig. 3 and Fig. 4 for both the strategies. It is evident from these plots that the convergence of rotor

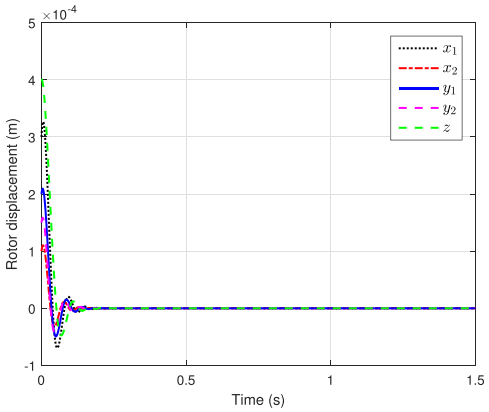

FIGURE 3. Trajectories of rotor positions under proposed ASNFTSMC scheme.

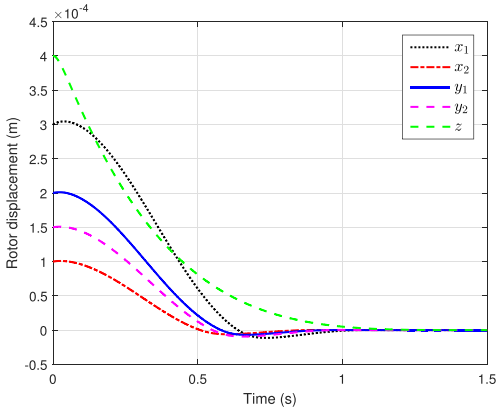

FIGURE 4. Trajectories of rotor positions under AISOSMC scheme.

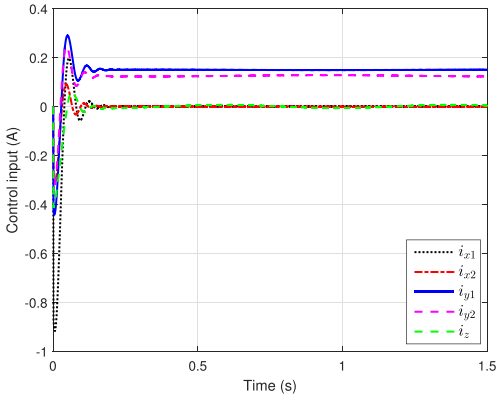

FIGURE 5. Control input response of the proposed scheme (19).

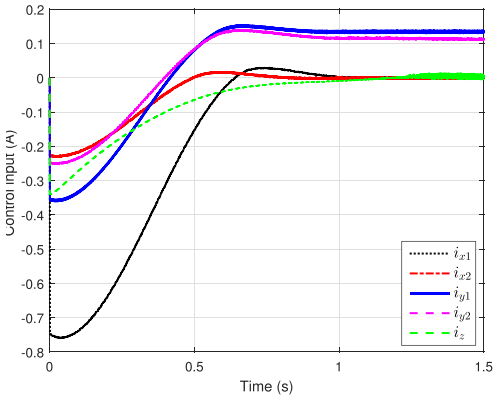

FIGURE 6. Control input response of AISOSMC.

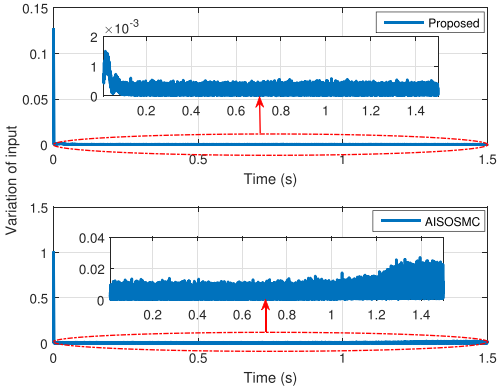

FIGURE 7. Time history of TV for both the schemes.

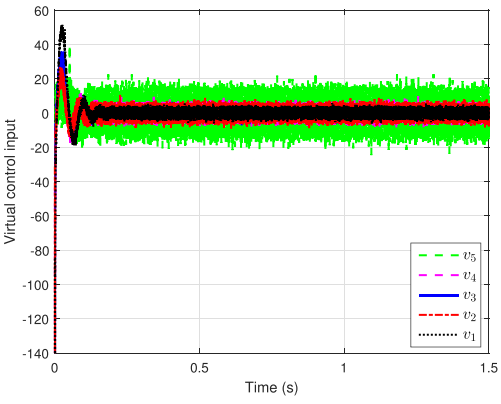

FIGURE 8. Time response of auxiliary control v(*t*) of ASNFTSMC.

position $\mathbf{x}$ to the neighborhood of origin under the proposed ASNFTSMC scheme is faster than the comparative AISOSMC scheme. Moreover, the settling time of $\mathbf{x}$ is measured when it converges to the bound $\|\mathbf{x}\| \leq 2 \times 10^{-6}$ m and stays within it. Hence, the calculated values of settling time (t_{settling}) under both cases are given in the performance measure Table 3, which also indicates that the proposed scheme is exhibiting a better response.

The transient and steady-state response of $\mathbf{x}$ is also measured via integral squared error (ISE), integral absolute error (IAE), integral time square error (ITAE), and integral time absolute error (ITAE). These performance indices are defined as [49]:

$$\text{ISE} = \int_{t_0}^{t} \left(\sum_{i=1}^{5} |x_i(\tau)|^2 \right) d\tau, \tag{48}$$

TABLE 3. Comparative performance measure of different control approaches.

Control Methodology	t_{settling} (s)	ISE (mm^3)	IAE (mm^2)	ITSE (mm^3s)	ITAE (mm^2s)	TV (A)	EI (A^2)
Proposed (19)	0.356	7.17×10^{-3}	3.79×10^{-2}	9.83×10^{-5}	1.16×10^{-3}	30.4	0.0841
AISOSMC [38]	1.186	7.22×10^{-2}	3.83×10^{-1}	1.11×10^{-2}	8.51×10^{-2}	745.9	0.2633

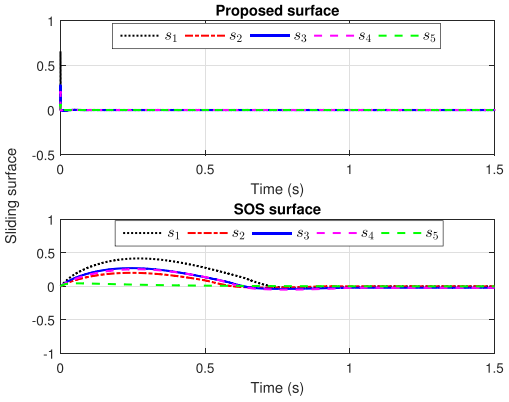

FIGURE 9. Trajectories of sliding surface under both SMC scheme.

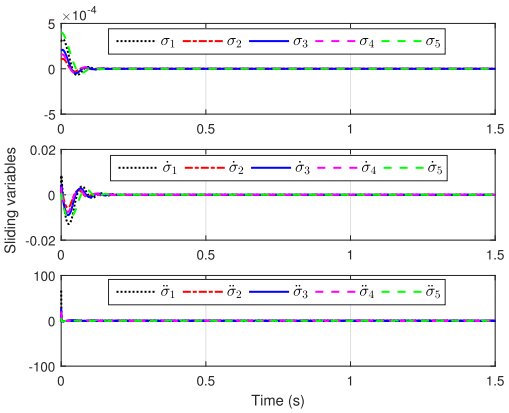

FIGURE 10. Trajectories of sliding variable under proposed ASNFTSMC scheme.

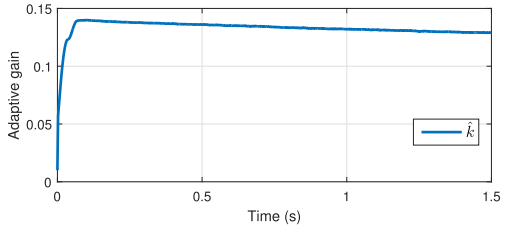

FIGURE 11. Response of adaptive gain under ASNFTSMC scheme.

$$\text{IAE} = \int_{t_0}^{t} \left(\sum_{i=1}^{5} |x_i(\tau)| \right) d\tau, \tag{49}$$

$$\text{ITSE} = \int_{t_0}^{t} \left(\sum_{i=1}^{5} \tau |x_i(\tau)|^2 \right) d\tau, \tag{50}$$

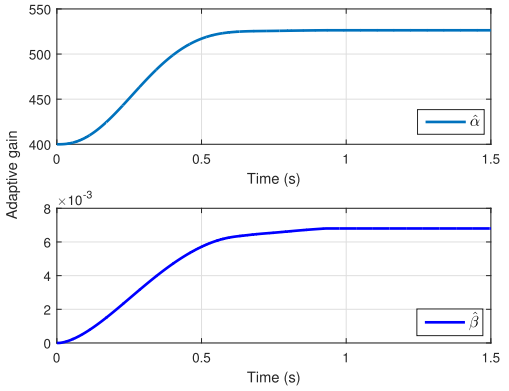

FIGURE 12. Response of adaptive gains under AISOSMC scheme.

$$\text{ITAE} = \int_{t_0}^{t} \left(\sum_{i=1}^{5} \tau |x_i(\tau)| \right) d\tau, \tag{51}$$

where t_0 and t are the initial and final time, respectively. The obtained values of ISE, IAE, ITSE, and ITAE under both the schemes are tabulated in Table 3. These performance results illustrate that the proposed ASNFTSMC algorithm achieves a better error response than the AISOSMC scheme.

The control input response of ASNFTSMC and AISOSMC scheme is presented in Fig. 5 and Fig. 6, respectively. The control input attains the steady-state around 0.4s under the proposed approach, and with the AISOSMC method, it is around 1s. In both control responses, there are two control components (i_{y_1}, i_{y_2}) that have non-zero steady-state values. This is because these corrective inputs are nullifying the effects of system uncertainties even when the rotor position reaches the nominal air gap location. Moreover, on close observation, one can notice that in Fig. 6, there is some chattering in the control input. Therefore, to quantify the amount of chattering, the total variation (TV) of control input is calculated, which is the summation over time of the absolute change in the present and the immediate past values of each control component. The expression of TV is given as

$$\text{TV} = \sum_{i=1}^{5} \sum_{j=0}^{n} |u_i(j+1) - u_i(j)|, \tag{52}$$

where n is the total number of iterations. The time-varying response of absolute input variation is illustrated in Fig. 7, and the value of TV under both SMC schemes is given in Table 3. Thus, the input variation plot (Fig. 7) and the TV values from Table 3 shows that the proposed ASNFTSMC methodology reduces the input chattering remarkably as compared to the algorithm of [38]. The performance of control input is also

compared in terms of energy consumption, and it is measured using an energy index (EI) function defining as:

$$\mathrm{EI} = \sum_{i=1}^{5} \int_{t_0}^{t} |u_i(\tau)|^2 \, d\tau. \tag{53}$$

The calculated value of EI is also given in Table 3 that corroborates that the proposed approach (19) is consuming less energy than AISOSMC method. The response of auxiliary control input $\mathbf{v}(t)$ is presented in Fig. 8. This plot illustrate that the chattering component of proposed control input is occurring in the derivative of actual input, i.e., $\mathbf{v}(t) = \dot{\mathbf{u}}(t)$. Hence, the actual control input $\mathbf{u}(t)$ is able to alleviate the high frequency component from its time response (as depicted in Fig. 5).

The time history of sliding surfaces of both schemes is presented in Fig. 9. The trajectories of the proposed second-order non-singular fast terminal sliding surface are shown on the top subplot of Fig. 9, and the second-order sliding surface of [38] is depicted at the bottom subplot. It is evident from these two surface responses that the proposed strategy achieves a faster sliding mode phase with a better convergence bound. As a result, the proposed scheme provides a stronger robustness characteristic. Furthermore, Fig. 10 presents the time response of sliding variables which are employed for the design of the proposed control algorithm. It can be observed from Fig. 10 that the variables $\boldsymbol{\sigma}$, $\dot{\boldsymbol{\sigma}}$, and $\ddot{\boldsymbol{\sigma}}$ are all converging to the neighborhood of zero around 0.4s. This implies that the higher order sliding variables are also effectively converging to zero under the proposed methodology.

The time-varying response of the proposed adaptive gain ($\hat{k}$) is plotted in Fig. 11. The adaptive gain settles to a value around 0.14 within 0.4 s. One thing to note is that the response of $\hat{k}$ is slowly decreasing once it reaches an appropriate gain value, and this is because of the governing equation of adaptation law (20). Therefore, when $\|\mathbf{s}\| \leq \bar{\epsilon}$ and $\hat{k} > \bar{\mu}$, the rate of $\hat{k}$ is decreasing in nature. Consequently, as $\mathbf{s}$ reaches to the steady state after 0.4 s, $\dot{\hat{k}}$ becomes less than zero. Hence, gain $\hat{k}$ starts decreasing marginally, as shown in Fig. 11. On the other hand, in AISOSMC [38], two adaptive gains are used, and their responses are depicted in Fig. 12. These adaptive estimates $\hat{\alpha}$ and $\hat{\beta}$ are settling to a value of around 527 and 6.8×10^{-3}, in 0.6 s and 0.9 s, respectively.

The above comparative study establishes that the proposed ASNFTSMC method has a faster response, better convergence bound with a preferable error performance measure, lesser energy consumption, and a better alleviation of input chattering.

VI. CONCLUSION

This paper investigates an adaptive second-order non-singular fast terminal SMC strategy for the five DOF AMB system to achieve faster response, finite-time convergence, and alleviation of input chattering. The adaptive gain relaxes restrictive assumptions about the bound disturbance and escapes the overestimation problem of switching gain. The stability analysis is proved through Lyapunov theory that guarantees the practical finite-time stability of the AMB system where the rotor position converges to a narrow bound in the vicinity of origin. The proposed methodology is also validated with a comparative study using simulation analysis. The numerical results illustrate the effectiveness of the proposed algorithm in terms of faster convergence, better transient and steady-state performances, reduction in input chattering, and lesser energy consumption. The future extension of the proposed work will incorporate more complexity in the AMB system, such as the rotor flexibilities and gyroscopic effects.

REFERENCES

[1] M. S. Kandil, M. R. Dubois, J. P. F. Trovão, and L. S. Bakay, "Application of second-order sliding-mode concepts to active magnetic bearings," *IEEE Trans. Ind. Electron*, vol. 65, no. 1, pp. 855–864, Jan. 2018.

[2] G. Schweitzer, "Active magnetic bearings-chances and limitations," in *Proc. 6th Int. Conf. Rotor Dyn.*, 2002, pp. 1–14.

[3] C. R. Knospe, "Active magnetic bearings for machining applications," *Control Eng. Pract.*, vol. 15, no. 3, pp. 307–313, Mar. 2007.

[4] G. Schweitzer and E. H. Maslen, *Magnetic Bearings: Theory, Design, and Application to Rotating Machinery*. Berlin, Germany: Springer, 2009.

[5] H. Bleuler, M. Cole, P. Keogh, R. Larsonneur, E. Maslen, Y. Okada, G. Schweitzer, and A. Traxler, *Magnetic Bearings: Theory, Design, and Application to Rotating Machinery*. Berlin, Germany: Springer, 2009.

[6] A. Tonoli, A. Bonfitto, M. Silvagni, L. D. Suarez, and F. Beltran-Carbajal, "Rotors on active magnetic bearings: Modeling and control techniques," in *Advances in Vibration Engineering and Structural Dynamics*. Rijeka, Croatia: InTech, 2012, pp. 1–27.

[7] K.-Y. Chen, P.-C. Tung, M.-T. Tsai, and Y.-H. Fan, "A self-tuning fuzzy PID-type controller design for unbalance compensation in an active magnetic bearing," *Expert Syst. Appl.*, vol. 36, no. 4, pp. 8560–8570, May 2009.

[8] L.-Y. Chang and H.-C. Chen, "Tuning of fractional pid controllers using adaptive genetic algorithm for active magnetic bearing system," *WSEAS Trans. Syst.*, vol. 8, no. 1, pp. 158–167, 2009.

[9] C. Bi, D. Wu, Q. Jiang, and Z. Liu, "Automatic learning control for unbalance compensation in active magnetic bearings," *IEEE Trans. Magn.*, vol. 41, no. 7, pp. 2270–2280, Jul. 2005.

[10] B. Polajžer, J. Ritonja, G. Štumberger, D. Dolinar, and J.-P. Lecointe, "Decentralized PI/PD position control for active magnetic bearings," *Elect. Eng.*, vol. 89, no. 1, pp. 53–59, Oct. 2006.

[11] S. Saha, A. Banerjee, S. M. Amrr, and M. U. Nabi, "Pseudospectral method-based optimal control for a nonlinear five degree of freedom active magnetic bearing system," *Trans. Inst. Meas. Control*, vol. 43, no. 7, pp. 1668–1679, Apr. 2021.

[12] M. O. Cole, C. Chamroon, and P. S. Keogh, "H-infinity controller design for active magnetic bearings considering nonlinear vibrational rotordynamics," *Mech. Eng. J.*, vol. 4, no. 5, 2017, Art. no. 00716.

[13] F. Carmo Carvalho, M. V. Fernandes de Oliveira, F. A. Lara-Molina, A. A. Cavalini, and V. Steffen, "Fuzzy robust control applied to rotor supported by active magnetic bearing," *J. Vibrat. Control*, vol. 27, nos. 7–8, pp. 912–923, Apr. 2021.

[14] V. Utkin, J. Guldner, and J. Shi, *Sliding Mode Control in Electro-Mechanical Systems*. Boca Raton, FL, USA: CRC Press, 2009.

[15] C. Edwards and S. Spurgeon, *Sliding Mode Control: Theory and Applications*. Boca Raton, FL, USA: CRC Press, 1998.

[16] M.-J. Jang, C.-L. Chen, and Y.-M. Tsao, "Sliding mode control for active magnetic bearing system with flexible rotor," *J. Franklin Inst.*, vol. 342, no. 4, pp. 401–419, 2005.

[17] M. S. Kang, J. Lyou, and J. K. Lee, "Sliding mode control for an active magnetic bearing system subject to base motion," *Mechatronics*, vol. 20, no. 1, pp. 171–178, Feb. 2010.

[18] F.-J. Lin, M.-S. Huang, and S.-Y. Chen, "Intelligent double integral sliding-mode control for five-degree-of-freedom active magnetic bearing system," *IET Control Theory Appl.*, vol. 5, no. 11, pp. 1287–1303, Jul. 2011.

[19] X. Yao and Z. B. Chen, "Sliding mode control with deep learning method for rotor trajectory control of active magnetic bearing system," *Trans. Inst. Meas. Control*, vol. 41, no. 5, pp. 1383–1394, Mar. 2019.
[20] S. Saha, S. M. Amrr, M. U. Nabi, and A. Iqbal, "Reduced order modeling and sliding mode control of active magnetic bearing," *IEEE Access*, vol. 7, pp. 113324–113334, 2019.
[21] Y. Shtessel, C. Edwards, L. Fridman, and A. Levant, *Sliding Mode Control and Observation*. New York, NY, USA: Springer, 2014.
[22] Q. Xu, "Precision motion control of piezoelectric nanopositioning stage with chattering-free adaptive sliding mode control," *IEEE Trans. Autom. Sci. Eng.*, vol. 14, no. 1, pp. 238–248, Jan. 2017.
[23] J.-J. E. Slotine and W. Li, *Applied Nonlinear Control*, vol. 199, no. 1. Englewood Cliffs, NJ, USAL Prentice-Hall, 1991.
[24] I. M. Boiko, "Chattering in sliding mode control systems with boundary layer approximation of discontinuous control," *Int. J. Syst. Sci.*, vol. 44, no. 6, pp. 1126–1133, Jun. 2013.
[25] A. Levant, "Higher-order sliding modes, differentiation and output-feedback control," *Int. J. Control*, vol. 76, nos. 9–10, pp. 924–941, Jan. 2003.
[26] J. Davila, L. M. Fridman, and A. Levant, "Second-order sliding-mode observer for mechanical systems," *IEEE Trans. Autom. Control*, vol. 50, no. 11, pp. 1785–1789, Nov. 2005.
[27] S. Saha, S. M. Amrr, A. S. Saidi, A. Banerjee, and M. Nabi, "Finite-time adaptive higher-order SMC for the nonlinear five DOF active magnetic bearing system," *Electronics*, vol. 10, no. 11, p. 1333, Jun. 2021.
[28] A. Levant, "Principles of 2-sliding mode design," *Automatica*, vol. 43, no. 4, pp. 576–586, 2007.
[29] M. Reichhartinger and M. Horn, "Application of higher order sliding-mode concepts to a throttle actuator for gasoline engines," *IEEE Trans. Ind. Electron.*, vol. 56, no. 9, pp. 3322–3329, Sep. 2009.
[30] A. Pisano, A. Davila, L. Fridman, and E. Usai, "Cascade control of PM DC drives via second-order sliding-mode technique," *IEEE Trans. Ind. Electron.*, vol. 55, no. 11, pp. 3846–3854, Nov. 2008.
[31] J. R. Dominguez, C. Mora-Soto, S. Ortega-Cisneros, J. J. R. Panduro, and A. G. Loukianov, "Copper and core loss minimization for induction motors using high-order sliding-mode control," *IEEE Trans. Ind. Electron.*, vol. 59, no. 7, pp. 2877–2889, Jul. 2012.
[32] P. M. Tiwari, S. Janardhanan, and M. un Nabi, "Attitude control using higher order sliding mode," *Aerosp. Sci. Technol.*, vol. 54, pp. 108–113, Jul. 2016.
[33] M. S. Kandil, P. Micheau, J. P. Trov ao, L. S. Bakay, and M. R. Dubois, "Hybrid magnetic bearing regulation via super twisting control," in *Proc. 15th Int. Conf. Control, Autom. Syst. (ICCAS)*, Oct. 2015, pp. 1566–1571.
[34] V. V. Huynh and B. D. Hoang, "Second order sliding mode control design for active magnetic bearing system," in *AETA 2015: Recent Advances in Electrical Engineering and Related Sciences*. Cham, Switzerland: Springer, 2016, pp. 519–529.
[35] S.-Y. Chen and F.-J. Lin, "Robust nonsingular terminal sliding-mode control for nonlinear magnetic bearing system," *IEEE Trans. Control Syst. Technol.*, vol. 19, no. 3, pp. 636–643, May 2011.
[36] H.-K. Chiang, C.-C. Fang, W.-B. Lin, and G.-W. Chen, "Second-order sliding mode control for a magnetic levitation system," in *Proc. 8th Asian Control Conf. (ASCC)*, May 2011, pp. 602–607.
[37] S. Jain, J. P. Mishra, and D. B. Talange, "A robust control approach for magnetic levitation system based on super-twisting algorithm," in *Proc. 10th Asian Control Conf. (ASCC)*, May 2015, pp. 1–6.
[38] S. Saha, S. M. Amrr, and M. Nabi, "Adaptive second order sliding mode control for the regulation of active magnetic bearing," *IFAC-PapersOnLine*, vol. 53, no. 1, pp. 1–6, 2020.
[39] S. Sivrioglu, "Adaptive backstepping for switching control active magnetic bearing system with vibrating base," *IET Control Theory Appl.*, vol. 1, no. 4, pp. 1054–1059, Jul. 2007.
[40] A. Abooee and M. M. Arefi, "Robust finite-time stabilizers for five-degree-of-freedom active magnetic bearing system," *J. Franklin Inst.*, vol. 356, no. 1, pp. 80–102, Jan. 2019.
[41] F. J. Lin, S. Y. Chen, and M. S. Huang, "Tracking control of thrust active magnetic bearing system via Hermite polynomial-based recurrent neural network," *IET Electr. Power Appl.*, vol. 4, no. 9, pp. 701–714, Nov. 2010.
[42] F. Plestan, Y. Shtessel, V. Brégeault, and A. Poznyak, "New methodologies for adaptive sliding mode control," *Int. J. Control*, vol. 83, no. 9, pp. 1907–1919, 2010.
[43] S. Singh, P. Srivastava, and S. Janardhanan, "Adaptive higher order sliding mode control for nonlinear uncertain systems," *IFAC-PapersOnLine*, vol. 51, no. 1, pp. 341–346, 2018.
[44] S. P. Bhat and D. S. Bernstein, "Finite-time stability of continuous autonomous systems," *SIAM J. Control Optim.*, vol. 38, no. 3, pp. 751–766, Jan. 2000.
[45] Z. Zhu, Y. Xia, and M. Fu, "Attitude stabilization of rigid spacecraft with finite-time convergence," *Int. J. Robust Nonlinear Control*, vol. 21, no. 6, pp. 686–702, Apr. 2011.
[46] S. M. Amrr, J. P. Srivastava, and M. Nabi, "Robust attitude stabilization of spacecraft under constrained network with hysteresis quantizer," *IEEE J. Miniaturization Air Space Syst.*, vol. 2, no. 3, pp. 129–139, Sep. 2021.
[47] A. Chakravarty and C. Mahanta, "Actuator fault-tolerant control (FTC) design with post-fault transient improvement for application to aircraft control," *Int. J. Robust Nonlinear Control*, vol. 26, no. 10, pp. 2049–2074, Jul. 2016.
[48] S. P. Bhat and D. S. Bernstein, "Geometric homogeneity with applications to finite-time stability," *Math. Control, Signals, Syst.*, vol. 17, no. 2, pp. 101–127, Jun. 2005.
[49] R. C. Dorf and R. H. Bishop, *Modern Control Systems*, 13th ed. London, U.K.: Pearson, 2017.

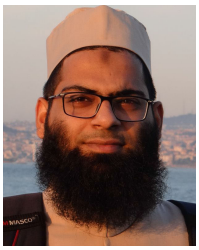

SYED MUHAMMAD AMRR (Graduate Student Member, IEEE) received the B.Tech. degree in electrical engineering and the M.Tech. degree in instrumentation and control from the Department of Electrical Engineering, Aligarh Muslim University (AMU), Aligarh, India, in 2014 and 2016, respectively, and the Ph.D. degree in control & automation from the Department of Electrical Engineering, Indian Institute of Technology Delhi (IITD), India, in 2021. He is currently a Postdoctoral Researcher with the Indian Institute of Technology Delhi (IITD). He has published more than 40 research papers in refereed international journals and conference proceedings. Further, an Australian Patent is also granted to his name, and he has authored a book chapter with CRC, Taylor and Francis, USA. His research interests include nonlinear control, sliding mode control, robust control, spacecraft systems, constrained network control system, renewable energy, and power electronics.

ABDULRAHMAN ALTURKI received the B.Sc. degree (Hons.) in electrical and communication engineering from Qassim University, Saudi Arabia, in 2008, and the M.Sc. and Ph.D. degrees in electrical engineering from the University of Dayton, Ohio, USA, in 2012 and 2017, respectively. He joined as an Assistant Professor with the Electrical Engineering Department, College of Engineering, Qassim University, in 2017. He has published several scientific papers in national and international conference proceedings and journals. His current research interests include computer vision, image restoration, multi-carrier communication systems, digital signal processing, digital communications, and channel equalization.